

# Structural and catalytic properties of skeletal Ni catalyst prepared from the rapidly quenched Ni<sub>50</sub>Al<sub>50</sub> alloy

Huarong Hu,<sup>a</sup> Minghua Qiao,<sup>a,\*</sup> Shuai Wang,<sup>a</sup> Kangnian Fan,<sup>a,\*</sup> Hexing Li,<sup>b</sup> Baoning Zong,<sup>c</sup> and Xiaoxin Zhang<sup>c</sup>

<sup>a</sup> Shanghai Key Laboratory of Molecular Catalysis and Innovative Materials, Department of Chemistry, Fudan University, Shanghai 200433, People's Republic of China

<sup>b</sup> Department of Chemistry, Shanghai Normal University, Shanghai 200234, People's Republic of China

<sup>c</sup> Research Institute of Petroleum Processing, Beijing 100083, People's Republic of China

Received 14 July 2003; revised 29 September 2003; accepted 30 September 2003

## Abstract

The textural and structural properties of a skeletal Ni catalyst prepared by alkali leaching of aluminum from the rapidly quenched Ni<sub>50</sub>Al<sub>50</sub> alloy have been investigated by elemental analysis (ICP-AES), nitrogen physisorption, powder X-ray diffraction (XRD), scanning electron microscopy (SEM), and H<sub>2</sub> thermal desorption techniques. As compared to Raney Ni, such a skeletal catalyst has a residual Ni<sub>2</sub>Al<sub>3</sub> phase, lower surface area, higher average pore diameter and porosity, larger mean crystallite size, and unit-cell parameter. These differences are attributable to the metastable character of the pristine rapidly quenched alloy and their relationship with the catalytic behavior is discussed and correlated.

© 2003 Published by Elsevier Inc.

**Keywords:** Rapid quenching; Ni–Al alloy; Skeletal catalyst; Raney Ni; Texture; Structure; Hydrogenation

## 1. Introduction

Since the introduction of the rapid quenching technique in production of metastable alloys with amorphous or nanocrystalline structure [1], these alloys have attracted the attention of metallurgists, physicists, and chemists due to their superior electronic, magnetic, mechanical, and chemical properties [2].

In catalysis, metastable alloys have been regarded as interesting from the point of view as follows: because of a lack of long-range ordering, the surface of metastable alloys is rich in low-coordination sites and defects which are essential for adsorption and activation of the reactants [3]. The catalytic activity of *amorphous* alloys was at first examined in the hydrogenation of carbon monoxide. A comparison of different amorphous Ni–Fe–metalloid alloys and their crystalline counterparts reveals that amorphous alloys have higher activity [4]. This pioneering finding has stimulated a variety of studies all over the world into the catalytic ac-

tivity and structural and electronic properties of amorphous alloys [2,5–9]. However, the fundamental knowledge of the textural and structural properties of the catalysts prepared from the rapidly quenched *nanocrystalline* alloys, another kind of metastable alloy, is really deficient, although several recent investigations have revealed their superior activity and selectivity in some hydrogenation reactions [10–14].

In this paper, we report a detailed characterization of a skeletal Ni catalyst (designated as RQ Ni) prepared by alkali dissolution of the rapidly quenched Ni<sub>50</sub>Al<sub>50</sub> alloy (Ni/Al, w/w, designated as RQ Ni–Al). Choosing this system is supported by the fact that Ni is one of the most commonly used catalysts in industry [15]. Furthermore, as the characteristics of Raney Ni are well known [16–22], it simplifies the interpretation of the effect of rapid quenching on the skeletal Ni catalyst. Based on elemental analysis, nitrogen physisorption, SEM, XRD, and H<sub>2</sub> desorption, we disclosed that under a typical alkali-leaching condition, skeletal Ni catalyst derived from the rapidly quenched Ni<sub>50</sub>Al<sub>50</sub> alloy shows comprehensive differences in phase composition, particle size, surface area, and porosity as compared to Raney Ni. Careful XRD analysis also reveals that the skeletal Ni catalyst has

\* Corresponding authors.

E-mail address: knfan@fudan.edu.cn (K. Fan).

larger mean crystallite size and lattice constant. The textural and structural differences are well correlated with the origin of the alloys. These results provide the preliminary information for the elucidation of the different catalytic behavior between the as-quenched skeletal Ni catalyst and conventional Raney Ni catalyst. Moreover, they may provide a basis for the interpretation of the catalytic behavior of rapidly quenched alloys other than the Ni–Al alloy.

## 2. Experimental

### 2.1. Catalyst preparation

The RQ Ni–Al alloy, containing an equal weight of metallic nickel and metallic aluminum with a purity of 99.99% and in the form of ribbons with a cross section of ca.  $0.02 \times 5 \text{ mm}^2$ , was prepared by a single roller melt-spinning method at a cooling rate of  $10^6 \text{ K s}^{-1}$ . Accurately weighed metallic Ni and Al specimens were melted at 1573 K under Ar atmosphere before it was sprayed onto the high-speed rotation copper wheel. The brittle ribbons were crushed and sieved, and the 200-mesh fraction was used throughout the experiments.

The RQ Ni catalyst was prepared by the following procedure: 1.0 g of RQ Ni–Al alloy was added under gentle stirring to an aqueous NaOH solution (10 ml, 6.0 M), heated to 363 K in a thermostated oil bath. After addition, the reaction system was kept on stirring at 363 K for 1.0 h for further alkali leaching. The black precipitate was washed with distilled water to neutrality and then with ethanol to replace water. The resulting catalyst was kept in a stoppered test tube under ethanol. Measurements were made within 24 h of catalyst preparation. Raney Ni catalyst was prepared by alkali leaching of a commercially available crystalline Ni–Al alloy (Ni/Al, 50/50, w/w, Shanghai Chemical Corp.) using the same procedure. It should be noted that as RQ Ni catalyst is pyrophoric, just like Raney Ni, during sample handling, care must be taken to preclude air oxidation.

### 2.2. Catalyst characterization

The bulk compositions of the leached samples (wt%) were analyzed by inductively coupled plasma-atomic emission spectroscopy (ICP-AES, Jarrell-Ash Atom Scan 2000). The surface morphologies were observed by scanning electron microscopy (SEM, Philips XL 30). Before being transferred into the SEM chamber, Raney or RQ Ni catalyst with ethanol was dispersed on the sample holder and then quickly moved into the vacuum evaporator (LDM-150D) in which a thin gold film was deposited after drying in vacuo.

The nitrogen isotherms and subsequently the multipoint Brunauer–Emmett–Teller (BET) surface areas ( $S_{\text{BET}}$ ) and the pore distributions of the samples were determined by  $\text{N}_2$  adsorption at 77 K in the Micromeritics TriStar 3000 apparatus, using a value of  $0.164 \text{ nm}^2$  for the cross section of the

nitrogen molecule. Samples were transferred to the adsorption glass tube with the storage liquid and treated at 383 K under ultrahigh pure nitrogen flow for 2.0 h before measurement. Samples were weighed by difference in the adsorption tube on completion of the experiment.

Powder X-ray diffraction (XRD) patterns were acquired on a Bruker AXS D8 Advance X-ray diffractometer using  $\text{Cu-K}\alpha$  radiation (0.15418 nm). The tube voltage and current was 40 kV and 40 mA, respectively. Sample with solvent was put in the in situ cell, with argon (99.9995%) flow purging the sample during the detection to avoid oxidation. The mean crystallite dimensions were obtained from the integral width of the Ni(111) diffraction line using the Scherrer relation after correction for instrumental broadening with the Warren procedure [23]. To obtain an estimate of the contribution to any given peak width by the instrumental factor, quartz powder was used due to its good crystalline perfection and virtually no intrinsic line broadening [19]. As nickel is face-centered cubic, mean unit-cell-parameter evaluations were made from the interplanar spacings calculated for all observed diffraction peaks by using the simple crystallographic relation between the two which holds for cubic structures.

$\text{H}_2$  desorption profiles were obtained in the following manner. After the samples were treated at 423 K for 1.0 h under argon flow (99.9995%, deoxygenated by an Alltech Oxy-trap filter), they were cooled down to room temperature before saturation chemisorption of hydrogen by pulsed injection as confirmed by the constant eluted peak area. The maximum desorption temperature, 650 K, was reached at a ramping rate of  $20 \text{ K s}^{-1}$ .

### 2.3. Activity test

Liquid-phase hydrogenations of 14 common organic molecules (cyclohexene, acrylonitrile, styrene, crotonaldehyde, cinnamaldehyde, glucose, cyclohexanone, acetophenone, 2-ethylanthraquinone, benzene, toluene, nitrobenzene, *p*-nitrophenol, and acetonitrile) were carried out in a 220 ml stainless-steel autoclave using Raney Ni and RQ Ni as the catalyst. The studied molecules contain one or more olefinic, aldehydic/ketonic, phenyl, nitril, and nitrile groups. The detailed reaction conditions were compiled in Table 2 for clarity. The hydrogenation process was monitored by sampling the reaction mixture at intervals, followed by gas or liquid chromatographic analysis based on the characteristics of the organic compounds. By fitting and differentiating the concentration-time curves of the reactant and the product, the initial hydrogenation rate of the reactant and the initial formation rate of the product were derived. Thus the turnover frequency (TOF) of the reactant and the selectivity to the target product if there were one more product can be obtained. All data were measured at least in triplicate.

### 3. Results

#### 3.1. Structural analysis of the pristine Ni–Al alloys

The X-ray diffraction patterns of the pristine RQ and Raney Ni–Al alloys are given in Fig. 1. The RQ Ni–Al alloy is composed of the  $\text{NiAl}_3$  and  $\text{Ni}_2\text{Al}_3$  phases [24], while for Raney Ni–Al alloy there is an additional diffraction peak at  $2\theta = 38.5^\circ$  characteristic of the eutectic phase having a nickel content of only about 5% [25]. A comparison of the intensities of the two lines at about  $25.4$  and  $25.9^\circ$ , corresponding to the  $\text{Ni}_2\text{Al}_3$  and  $\text{NiAl}_3$  phases, respectively, directly leads to the conclusion that the relative molar ratio of  $\text{NiAl}_3$  to  $\text{Ni}_2\text{Al}_3$  in RQ Ni–Al alloy is higher than in Raney Ni–Al alloy.

By a simple calculation, the weight percents of aluminum in the  $\text{NiAl}_3$  and  $\text{Ni}_2\text{Al}_3$  phases are 57.97 and 40.81%, respectively. Thus the relatively higher content of the  $\text{NiAl}_3$  phase compensates for the lack of the eutectic in the RQ Ni–Al alloy. A microscopic interpretation of the difference between these two XRD patterns can be depicted as follows. For RQ Ni–Al alloy, as the solidification speed is extremely high, the advance of the liquid–solid interface is so fast that it depresses the long-range diffusion of the atoms and consequently the formation of the phases with composition substantially deviating from the alloy average composition, e.g., the eutectic. In addition, under the supercooling condition as the nucleation speed is much faster than the growth rate, it leads to more nuclei and finer crystallites, which is clearly evidenced by the broader diffraction lines for RQ Ni–Al alloy shown in Fig. 1.

#### 3.2. Characterization of the skeletal Ni samples

The nitrogen isotherms for RQ Ni and Raney Ni samples are shown in Fig. 2. Surface areas, pore volumes, and

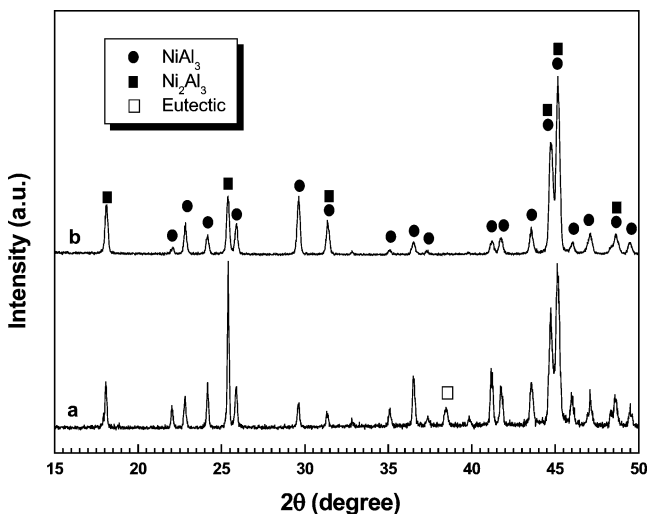


Fig. 1. XRD profiles of (a) Raney Ni–Al alloy and (b) rapidly quenched Ni–Al alloy.

Table 1

Physicochemical characters of the RQ Ni and Raney Ni catalysts

Catalyst	Composition (wt%)	$S_{\text{BET}}$ ( $\text{m}^2 \text{g}^{-1}$ )	$V_{\text{pore}}$ ( $\text{cm}^3 \text{g}^{-1}$ )	$d_{\text{pore}}$ (nm)	$d_{\text{cryst}}^a$ (nm)	$d_{\text{cell}}^b$ (nm)
Raney Ni	$\text{Ni}_{91.2}\text{Al}_{8.8}$	114	0.0911	3.422	5.2	0.3525
RQ Ni	$\text{Ni}_{89.6}\text{Al}_{10.4}$	106	0.1211	4.859	6.4	0.3548

<sup>a</sup> Mean crystallite size.

<sup>b</sup> Mean unit-cell dimension.

mean pore diameters for these samples calculated from the isotherms are listed in Table 1. The isotherms, being Type A according to de Boer's classification [26], indicate the open-ended cylindrical pore shape for both samples. The pore-size distributions of the samples are illustrated in Fig. 3. For Raney Ni catalyst, it exhibits a bimodal distribution with

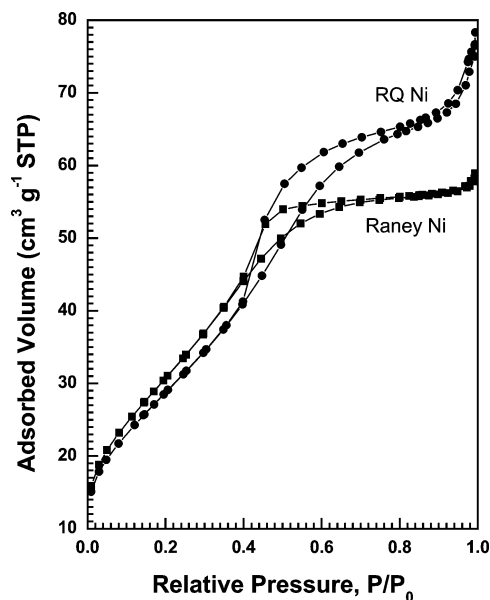


Fig. 2. Nitrogen isotherms at 77 K for Raney Ni and RQ Ni catalysts.

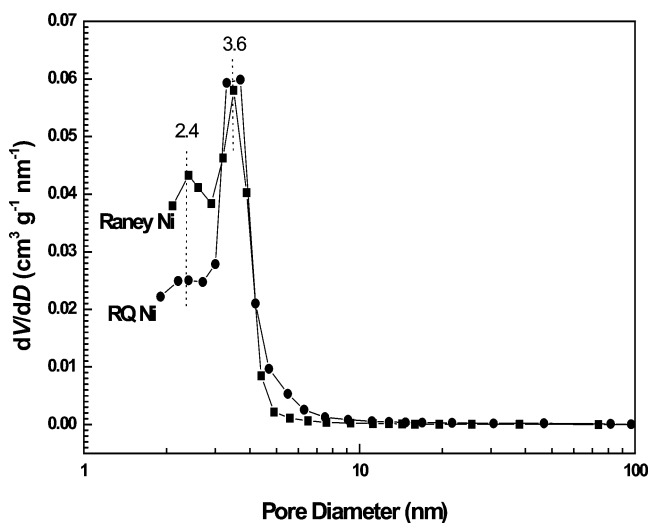


Fig. 3. Pore-size distribution of Raney Ni and RQ Ni catalysts calculated by the BJH equation in desorption branch.

maxima at pore diameters 2.4 and 3.6 nm from the desorption isotherm. The mean pore diameter from the ratio of pore volume to area for cylindrical pores is 3.422 nm and the pore volume is  $0.0911 \text{ cm}^3 \text{ g}^{-1}$ . The characteristics of Raney Ni catalyst are consistent with previous work [16]. On the other hand, the pore distribution for RQ Ni catalyst shows a small maximum or plateau at small diameters, followed by a large broad maximum. These features occur at similar pore diameters compared to Raney Ni catalyst. The mean diameter from the volume-to-area ratio is 4.859 nm and the pore volume is  $0.1211 \text{ cm}^3 \text{ g}^{-1}$ . Although the RQ Ni catalyst has a higher pore volume, its surface area is about  $8 \text{ m}^2 \text{ g}^{-1}$  lower than that observed for Raney Ni (because the RQ form exhibits a larger mean pore size). Similar phenomenon has also been reported for  $\text{Ni}_{52.5}\text{Al}_{47.5}$  [27] and  $\text{Cu}_{30}\text{Al}_{70}$  [28] alloys prepared by the melt-spinning method and in a conventional way.

Fig. 4 shows the SEM morphologies of the studied catalysts. It is observed that after aluminum leaching the smooth alloy surface becomes highly fractured, which contributes partly to the three orders of magnitude increment of the surface area. Furthermore, the surface morphologies of the leached samples (Figs. 4b and 4c) emphasize vividly the round and angular topographies of RQ Ni and Raney Ni particles, respectively, demonstrating their different origin. From the SEM graphs, it is found that the particle size of RQ Ni catalyst (ca.  $1 \mu\text{m}$ ) is smaller than that of Raney Ni (ca.  $5 \mu\text{m}$ ), while XRD will reveal a bigger crystallite size of the former in the following context.

The XRD profile of Raney Ni (Fig. 5a) exhibits the features at  $2\theta = 44.0, 51.2$ , and  $75.5^\circ$ , corresponding to metallic Ni (111), (200), and (222) planes, respectively, [24]. However, additional diffractions at  $44.2, 65.6$ , and  $83.0^\circ$ , corresponding to residual  $\text{Ni}_2\text{Al}_3$  (110), (202), and (212) planes, respectively, are evident for the RQ Ni catalyst (Fig. 5b), implying that the  $\text{Ni}_2\text{Al}_3$  phase in the rapidly quenched Ni–Al alloy is more difficult to be leached than that in the Raney Ni–Al alloy. The existence of a residual  $\text{Ni}_2\text{Al}_3$  phase has also been noted for leaching similar as-quenched Ni–Al [10] and Ni–P–Al alloys [13]. According to Fig. 1 and the experimental fact that the eutectic is much more reactive toward alkali than the  $\text{NiAl}_3$  and  $\text{Ni}_2\text{Al}_3$  phases [22,29,30], the eutectic of dendritic structure can immediately leave voids on dissolution [20], rendering efficient alkali diffusion into the interior of the alloy and consequently a more complete leaching of aluminum in the crystallites. An alternative may be that the rapid quenching technique leads to a  $\text{Ni}_2\text{Al}_3$  phase with nonstoichiometric composition [31] which is less vulnerable to alkali attack, as metastable alloys are generally considered to have superior corrosion resistance [2].

The mean crystallite sizes and unit-cell parameters for both samples derived from the XRD patterns are listed in Table 1. The crystallite size of RQ Ni catalyst (ca.  $6.4 \text{ nm}$ ) is remarkably larger than that of Raney Ni (ca.  $5.2 \text{ nm}$ ), while the latter is within the range for Raney Ni samples leached

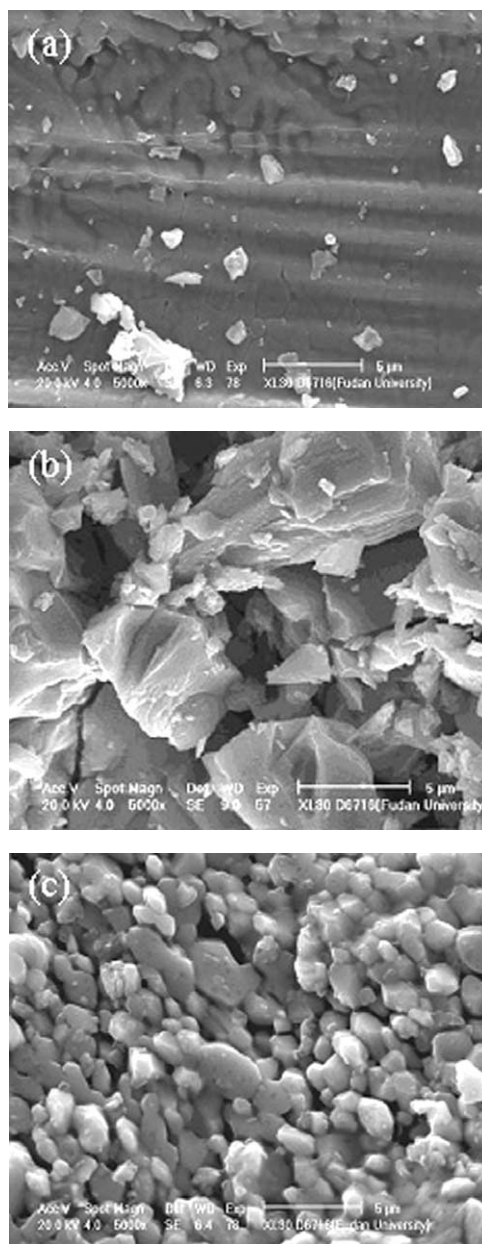


Fig. 4. SEM images of (a) pristine rapidly quenched Ni–Al alloy, (b) Raney Ni catalyst, and (c) RQ Ni catalyst.

by different ways [19]. The unit-cell dimension for nickel in Raney Ni is  $0.3525 \text{ nm}$ , close to the value for crystalline Ni of  $0.35238 \text{ nm}$  [32]. For comparison, Robertson et al. reported values from  $0.3528$  to  $0.3535 \text{ nm}$  for Raney Ni [19]. However, the value for RQ Ni catalyst is  $0.3548 \text{ nm}$ , significantly larger than the values reported above. Presumably, between the larger structural units exist larger voids; consequently, the sample with larger crystallites has a smaller surface area.

There is also difference in the  $\text{H}_2$  desorption profiles between the two samples. In Fig. 6, the Raney Ni catalyst shows two  $\text{H}_2$  desorption peaks at  $400$  and  $507 \text{ K}$  with

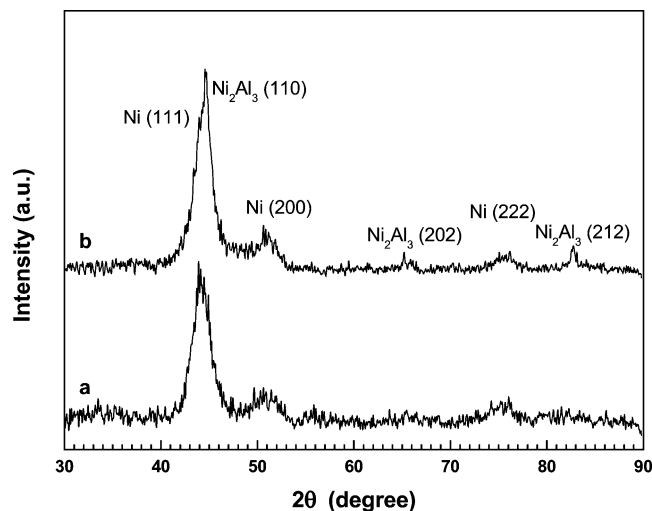


Fig. 5. XRD profiles of (a) Raney Ni catalyst and (b) RQ Ni catalyst.

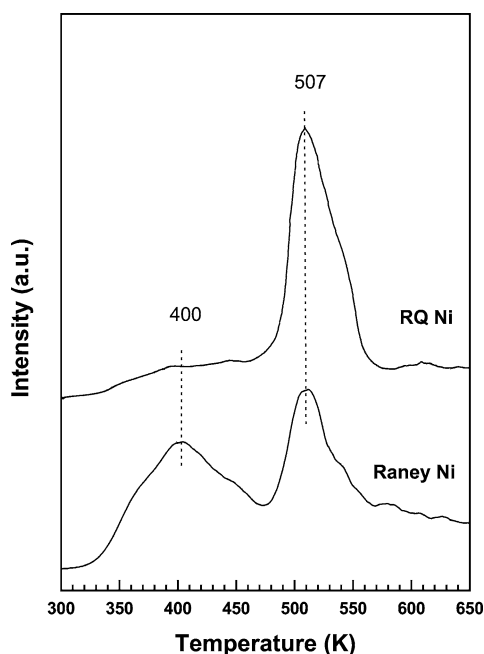


Fig. 6. The H<sub>2</sub> TPD features over Raney Ni and RQ Ni catalysts.

similar intensity, respectively. This agrees with the work by Serra et al. in both the desorption temperature and the relative intensity [33]. In contrast, for RQ Ni catalyst the high-temperature peak is much more intense than the low-temperature one, although the temperatures of the desorption maxima are similar to those of Raney Ni.

### 3.3. Catalytic performance

Table 2 summarizes the TOF values and selectivities, if there is more than one product determined chromatographically, over Raney Ni and RQ Ni catalysts in the liquid-phase hydrogenation of the above-noted unsaturated compounds. It is found that for olefinic (entries 1–5), carbonyl (entries 6–9), and nitril (entries 12–14) group hydrogenation,

RQ Ni catalyst is about 30 to 290% more active than Raney Ni. The rapid quenching technique is less effective in enhancing the phenyl group hydrogenation (entries 10 and 11); however, RQ Ni catalyst is still about 50 to 70% more active than Raney Ni. If the discrepancy in activity toward isolated groups is still held when two or more unsaturated groups coexist in one molecule, over RQ Ni catalyst a higher selectivity toward product with an intact phenyl moiety is expected. It is true that for bifunctional molecules such as styrene, acetophenone, and 2-ethylanthraquinone (entries 3, 8, and 9), the selectivities to ethylbenzene, 1-phenyl ethanol, and 2-ethylanthrahydroquinone, respectively, are no less than 90 mol% over RQ Ni catalyst. For  $\alpha$ ,  $\beta$ -unsaturated aldehyde hydrogenation (entries 4 and 5), formation of the saturated aldehydes (butanal and hydrocinnamaldehyde) is favored over RQ Ni, suggesting an enhanced reactivity of the olefinic group over the RQ Ni catalyst.

## 4. Discussion

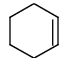
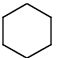
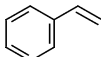
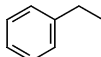
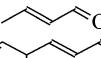
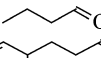
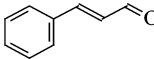
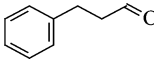
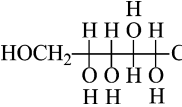
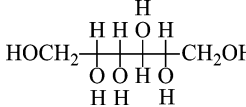
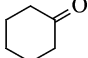
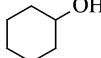
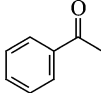
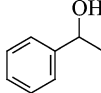
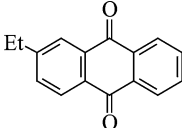
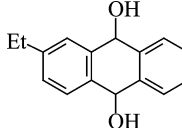
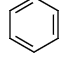
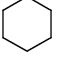
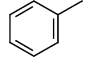
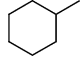
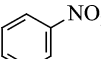
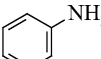
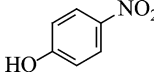
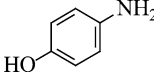
The phase selection of the rapidly quenched Ni–Al alloy is determined not only by the nucleation rate but also by the growth velocity of the crystallite, according to the nucleation theory and dendrite growth model out of the scope of the present study [34,35]. It is found that the Ni<sub>2</sub>Al<sub>3</sub> phase nucleates earlier upon cooling; however, the NiAl<sub>3</sub> phase will nucleate soon after the appearance of the Ni<sub>2</sub>Al<sub>3</sub> phase due to the extremely high cooling rate. Thus competitive growth between these two phases occurs. On the other hand, the nucleation and growth of the Ni<sub>2</sub>Al<sub>3</sub> phase lead to a liquid with composition much nearer to that of the NiAl<sub>3</sub> phase, which is favorable for the growth of the latter, as short-range diffusion rather than the long-range diffusion of the atoms dominates under the rapid quenching condition [36]. This may account for the relatively higher NiAl<sub>3</sub> content in the pristine RQ Ni–Al alloy than in the usual Raney Ni–Al alloy as revealed by Fig. 1.

When studying the effect of preparation parameters on the pore structure of Raney Ni, Freel and co-workers concluded that samples prepared under mild conditions have, in general, high surface area and narrow pores, while the samples after a severe leaching process are low-area materials with larger pores [16]. It is suggested that the migration of alumina trihydrate partially blocking and filling pores and the sintering of the crystallites change the pore structure to that typical of high-temperature extraction.

Based on our results as well as the cases of the quenched Ni<sub>52.5</sub>Al<sub>47.5</sub> and Cu<sub>30</sub>Al<sub>70</sub> alloys, the removal of alumina trihydrate does not seem to be the key factor to result in the difference of the pore structure, as the concentration of the alkali, the temperature, and reaction time when leaching the rapidly quenched and the Raney alloys are identical. Moreover, when preparing Raney Ni catalyst, the removal of alumina cannot account for the decrease of the surface area when the leaching time is prolonged, as more alumina

Table 2

The catalytic behaviors of RQ Ni and Raney Ni in hydrogenation of some unsaturated organic compounds

Entry	Substrate	Reaction conditions Sub. (mol)/Sol. (ml)/ $W_{\text{cat}}$ (g)/Temp. (K)/ $P_{\text{H}_2}$ (MPa)	Product	Selectivity (mol%)		TOF ( $\text{s}^{-1}$ )	
				Raney Ni	RQ Ni	Raney Ni	RQ Ni
1		0.0986/cyclohexane, 30/0.20/323/1.0		–	–	0.40	0.91
2	$\text{CH}_2=\text{CHCN}$	0.0760/ethanol, 45/0.20/323/1.0	$\text{CH}_3\text{CH}_2\text{CN}$	–	–	0.20	0.59
3		0.0427/cyclohexane, 45/0.20/363/1.0		47.0	90.0	0.010	0.023
4		0.0611/ethanol, 45/0.20/323/0.80		82.4	96.2	0.84	1.5
5		0.0397/ethanol, 45/0.50/303/0.80		69.2	80.1	0.10	0.15
6		0.0694/water, 37.5/0.20/373/4.0		–	–	0.012	0.024
7		0.0815/cyclohexane, 30/0.20/363/3.0		–	–	0.061	0.24
8		0.0416/ethanol, 45/0.50/353/2.0		74.5	92.7	0.13	0.26
9		0.0148/mixture, <sup>a</sup> 70/0.50/323/0.30		51.2	96.6	0.023	0.030
10		0.256/cyclohexane, 25/0.20/363/4.0		–	–	0.16	0.24
11		0.0941/cyclohexane, 30/0.20/373/3.0		–	–	0.083	0.14
12		0.0977/ethanol, 30/0.20/363/2.0		–	–	0.26	0.59
13		0.0288/water, 40/0.20/353/2.0		–	–	0.056	0.13
14	$\text{CH}_3\text{C}\equiv\text{N}$	0.190/ethanol, 30/0.20/363/1.0	$\text{CH}_3\text{CH}_2\text{NH}_2$	–	–	0.16	0.56

<sup>a</sup> A mixture of trioctylphosphate and trimethylbenzene (volume ratio 3/7) was used as solvent.

should be leached out [16]. Thus, sintering of the crystallites is more likely to be accountable for the texture difference. Remember that due to rapid quenching, more defects are formed in the alloy. Crystallites obtained from the rapidly quenched alloy are coordinatively unsaturated and inclined to form larger grains, leading to catalysts with smaller surface area and larger pore size. This interpretation is rationalized by the bigger crystallite size of RQ Ni catalyst than that of Raney Ni from XRD analysis listed in Table 1.

On the other hand, Fig. 5 shows that there is residual  $\text{Ni}_2\text{Al}_3$  phase in RQ Ni catalyst, while this phase is indiscernible in Raney Ni. The remaining  $\text{Ni}_2\text{Al}_3$  phase can stabilize the skeleton, inhibiting the collapse of the pores [37], which may also contribute to the textural difference between RQ and Raney Ni catalysts. One should note that the existence of aluminum does not necessarily mean a poor

catalytic behavior. Fouilloux has observed that residual aluminum in Raney Ni catalyst is responsible for increasing the hydrogenation activity in certain reactions [22]. The higher catalytic activity of RQ Ni, as shown in Table 2, can be partly attributed to a similar effect. It is worthwhile to point out that the preparation of Raney Ni of large pore size and volume is always at the expense of the loss of aluminum [16], while it is not the case for skeletal Ni catalyst prepared from the rapidly quenched alloy.

The  $\text{H}_2$  desorption profiles in Fig. 6 show that the population of the weakly bound hydrogen is remarkably lower than the strongly bound hydrogen over RQ Ni catalyst, while they are comparable over Raney Ni. These results infer that the active sites over RQ Ni catalyst are more uniform, which may lessen the adsorption modes of the reactant and depress the occurrence of the side reactions. On the other hand,

a correlation of the binding strength of the chemisorbed hydrogen with the activity and selectivity for certain reactions has been successfully established by some authors [33,38–41]. For example, Mikhailenko et al. found that the relative amount of the weakly and strongly bound hydrogen determines the selectivity of 2-ethylanthraquinone hydrogenation [41], since the weakly bound hydrogen is highly reactive in aromatic ring hydrogenation, while the hydrogenation of carbonyl groups is caused by an electronic mechanism and is limited by hydrogen activation [42]. In Table 2 we have unambiguously verified that RQ Ni can be a promising alternative in 2-ethylanthraquinone selective hydrogenation, the key reaction for hydrogen peroxide production.

At this time, we are not very clear about the physics underlying the different H<sub>2</sub> desorption profiles. According to the XRD results, we tentatively attribute it to the more defective character of RQ Ni catalyst inherited from the rapidly quenched alloy. The expansion of the lattice constant of RQ Ni as compared to that of Raney Ni is expected to bond tightly with hydrogen. On the other hand, Balandin suggested that the dissociation of a reacting molecule, which is a necessary step for any catalytic reaction, is possible only if there exists a good match between the interatomic distances in this molecule and the atomic arrangement of the superficial metal atoms [43]. The increment of the lattice constant of RQ Ni catalyst, as a consequence of the increment of the Ni–Ni distance, thus has a pronounced influence on the activity and selectivity in certain reactions exemplified in Table 2.

## 5. Conclusions

This work presents a detailed study of the effect of rapid quenching on the physicochemical properties of the skeletal Ni catalyst. Under a typical alkali leaching condition, RQ Ni catalyst prepared from the rapidly quenched Ni<sub>50</sub>Al<sub>50</sub> alloy exhibits remarkable differences in phase composition, particle size, surface area, pore-size distribution, porosity, and H<sub>2</sub> desorption profile as compared to Raney Ni. Moreover, RQ Ni catalyst has a larger mean crystallite size and unit-cell parameter. The textural and structural differences are considered to be inherited from the pristine metastable alloy and have comprehensive influences on the catalytic behavior of skeletal Ni catalysts.

## Acknowledgments

This work is supported by the Major State Basic Research Development Program (G2000048009), the National Natural Science Foundation of China (20203004, 20073008), and the Natural Science Foundation of Shanghai Science and Technology Committee (02ZA14006).

## References

- [1] K. Klement, R.H. Willens, P. Duwez, *Nature* 187 (1960) 869.
- [2] Á. Molnár, G.V. Smith, M. Bartók, *Adv. Catal.* 36 (1989) 329.
- [3] G.A. Somorjai, *Catal. Rev. Sci. Eng.* 18 (1978) 173.
- [4] A. Yokoyama, H. Komiyama, H. Inoue, T. Masumoto, H. Kimura, *J. Catal.* 68 (1981) 355.
- [5] R. Schloegl, in: S. Steeb, H. Warlimont (Eds.), *Rapidly Quenched Metals*, Elsevier, Amsterdam, 1985, p. 1723.
- [6] C. Yoon, D.L. Cocke, *J. Non-Cryst. Solids* 79 (1986) 217.
- [7] M. Shibata, T. Masumoto, in: B. Delmon, P. Grange, P.A. Jacobs, G. Poncelet (Eds.), *Preparation of Catalysis IV*, Elsevier, Amsterdam, 1987, p. 353.
- [8] A. Baiker, *Faraday Discuss.*, Chem. Soc. 87 (1989) 239.
- [9] K. Hashimoto, *Mater. Sci. Eng. A* 226–228 (1997) 891.
- [10] Z.L. Lu, R. Wang, J. Ke, H. Chen, X.H. Mu, B.N. Zong, *Chin. J. Catal.* 18 (1997) 110.
- [11] H. Warlimont, U. Kühn, N. Mattern, *Mater. Sci. Eng. A* 226–228 (1997) 900.
- [12] H.X. Li, W.J. Wang, J.F. Deng, *J. Catal.* 191 (2000) 257.
- [13] H. Lei, Z. Song, D.L. Tan, X.H. Bao, X.H. Mu, B.N. Zong, E.Z. Min, *Appl. Catal. A* 214 (2001) 69.
- [14] B. Liu, M.H. Qiao, J.F. Deng, K.N. Fan, X.X. Zhang, B.N. Zong, *J. Catal.* 204 (2001) 512.
- [15] P.N. Rylander, *Ullmann's Encyclopedia of Industrial Chemistry*, Vol. A.13, VCH, Weinheim, 1989.
- [16] J. Freel, W.J.M. Pieters, R.B. Anderson, *J. Catal.* 14 (1969) 247.
- [17] J. Freel, W.J.M. Pieters, R.B. Anderson, *J. Catal.* 16 (1970) 281.
- [18] J. Freel, S.D. Robertson, R.B. Anderson, *J. Catal.* 18 (1970) 243.
- [19] S.D. Robertson, R.B. Anderson, *J. Catal.* 23 (1971) 286.
- [20] S.D. Robertson, R.B. Anderson, *J. Catal.* 41 (1976) 405.
- [21] S.D. Robertson, J. Freel, R.B. Anderson, *J. Catal.* 24 (1972) 130.
- [22] P. Fouilloux, *Appl. Catal.* 8 (1983) 1.
- [23] B.E. Warren, *J. Appl. Phys.* 12 (1941) 375.
- [24] PDFMaint Version 3.0, Powder diffraction database, Bruker Analytical X-ray systems GmbH, 1997.
- [25] P. Nash, *Phase Diagrams of Binary Nickel Alloys*, American Society for Metals, Materials Park, OH, 1991, p. 5.
- [26] J.H. de Boer, in: D.H. Everett, F.S. Stone (Eds.), *The Structure and Properties of Porous Materials*, Butterworth, London, 1958, p. 68.
- [27] X.M. Chen, G.S. Zhang, X.K. Wang, N.F. Shen, J. Zhengzhou, *Univ. Tech.* 20 (1999) 57.
- [28] L. Sun, Q.H. Song, Z.Q. Hu, *Acta Metall. Sin.* 32 (1996) 63.
- [29] R. Sassoulas, Y. Trambouze, *Bull. Soc. Chim. Fr.* 5 (1964) 985.
- [30] S. Sane, J.M. Bonnier, J.P. Damon, J. Masson, *Appl. Catal.* 9 (1984) 69.
- [31] A. Taylor, N.J. Doyle, *J. Appl. Crystallogr.* 5 (1972) 210.
- [32] H.E. Swanson, E. Fuyat, *Natl. Bur. Stand. Circ.* 1 (1953) 13.
- [33] M. Serra, P. Salagre, Y. Cesteros, F. Medina, J.E. Sueiras, *J. Catal.* 209 (2002) 202.
- [34] H. Assadi, M. Barth, A.L. Greer, D.M. Herlach, *Acta Mater.* 46 (1998) 491.
- [35] F.H. Ba, N.F. Shen, *Acta Metall. Sin.* 37 (2001) 845.
- [36] M.J. Aziz, *J. Appl. Phys.* 53 (1982) 1158.
- [37] M.L. Bakker, D.J. Young, M.S. Wainwright, *J. Mater. Sci.* 23 (1988) 3921.
- [38] P. Marécot, E. Paraiso, J.M. Dumas, J. Barbier, *Appl. Catal.* 74 (1991) 261.
- [39] S. Smeds, T. Salmi, L.P. Lindfors, O. Krause, *Appl. Catal. A* 114 (1996) 177.
- [40] Y. Cesteros, P. Salagre, F. Medina, J.E. Sueiras, *Appl. Catal. B* 25 (2000) 213.
- [41] S.D. Mikhailenko, A.B. Fasman, N.A. Maksinova, E.V. Leongard, *Appl. Catal.* 12 (1984) 141.
- [42] J.D. Roberts, M.C. Caserio, *Basic Principles of Organic Chemistry*, Benjamin, Redwood City, CA, 1964.
- [43] A.A. Balandin, *Z. Phys. Chem.* 132 (1929) 289.